JOURNAL OF PROPULSION AND POWER
Vol. 27, No. 2, March–April 2011

Heat Release in Turbine Cooling I: Experimental and Computational Comparison of Three Geometries

Marc D. Polanka,* Joseph Zelina,* Wesly S. Anderson,† and Balu Sekar*
U.S. Air Force Research Laboratory, Wright-Patterson Air Force Base, Ohio 45433
Dave S. Evans‡
Air Force Institute of Technology, Wright-Patterson Air Force Base, Ohio 45433
Cheng-Xian Lin§
University of Tennessee, Knoxville, Tennessee 37996
and
Scott D. Stouffer¶
University of Dayton Research Institute, Wright-Patterson Air Force Base, Ohio 45433

DOI: 10.2514/1.45317

The ultracompact combustor is a design that integrates a turbine vane into the combustor flowpath. Because of the high fuel-to-air ratio and short combustor flowpath, a significant potential exists for unburned fuel to enter the turbine. The current study explores the interaction of cooling flow from typical cooling holes with this high-temperature fuel-rich freestream flow. This was supplemented with a Reynolds-averaged Navier–Stokes calculation using a simplified two-step propane–air reaction scheme to model the combustion process and study the underlying physics of mixing between film-cooling and cross-stream-flow-driving secondary combustion. Results from surface temperature and heat flux measurements demonstrate that reactions in the turbine-cooling film can result in substantial increases in wall temperature for a considerable distance downstream of the hole. This increase depends on hole geometry, blowing ratio, and fuel content of the combustor flow. Furthermore, the heat flux increase only occurs when air is used as the coolant, as oxygen is needed to feed secondary combustion for the unburned fuel exiting the combustor at high equivalence ratios. Failure to design for this effect could result in augmented heat flux caused by the cooling scheme, and turbine life could be degraded substantially.

Nomenclature

A	=	area, m^2
a_0, a_1	=	curve fit parameter
C	=	constant of integration
D	=	diameter, m
k	=	thermal conductivity, $W/m^2 \cdot K$
L	=	total length, m
M	=	blowing ratio
$\dot{m}$	=	mass flow rate, g/ min; g/s
q''	=	heat flux, W/m^2
T	=	temperature, K
U	=	velocity, m/s
x	=	location; distance, m
η	=	adiabatic effectiveness
ρ	=	density, kg/m^3
Φ	=	equivalence ratio

Subscripts

c	=	coolant; convection
f	=	film
max	=	maximum
w	=	wall
x	=	depth, m
4	=	turbine inlet condition
∞	=	freestream; reactor exhaust stream

Presented as Paper 2009-0298 at the 47th AIAA Aerospace Sciences Meeting, Orlando, FL, 5–8 January 2009; received 6 May 2009; revision received 12 September 2010; accepted for publication 21 September 2010.

*Senior Research Engineer. Associate Fellow AIAA.
†Engineer.
‡Graduate Student. Student Member AIAA.
§Associate Professor. Senior Member AIAA.
¶Senior Research Engineer. Senior Member AIAA.

I. Introduction

THE thermal efficiency and specific thrust of gas turbine engines increase with increasing turbine inlet temperature T_4. The maximum allowable T_4, $T_{4\,\max}$, in practical engines is limited to those temperatures below which material failure or unacceptable reductions in service life are likely to occur. Gas turbine designs have shown a continued increase in $T_{4\,\max}$ since the invention of the gas turbine engine [1]. Because of the requirements to increase fuel efficiency and performance of aeronautical engines, designers will continue to push toward higher $T_{4\,\max}$. For decades, $T_{4\,\max}$ has exceeded the temperatures that would cause material failure of the turbine components [2]. To keep these components from failing and to extend their life, they have been cooled with air bled from the compressor. Initially, these components were cooled from the inside by a flow of bleed air through passages cut in the turbine blades. Later, turbines were designed to allow bleed air to be forced out through the turbine surfaces, forming a cooling film along the surface. Although this bleed air may locally increase the heat-transfer coefficient, the film serves to decrease the high temperatures that turbine surfaces contact and, if correctly designed, decreases the overall heat load to the part.

Historically, the combustion sections of gas turbine engines have operated at overall equivalence ratios Φ much less than one [3]. The definition of Φ is given in Eq. (1):

$$\Phi = \frac{(\dot{m}_{\text{fuel}}/m_{\text{air}})}{(\dot{m}_{\text{fuel}}/m_{\text{air}})_{\text{stoich}}} \tag{1}$$

Additionally, a relatively long flowpath within the combustor, on the order of 25–50 cm, compared with chemical and mixing times

ensured that reactions were complete before leaving the combustor. Therefore, there have been few unburned species entering the turbine. However, the desire to increase efficiency has led to the development of combustion sections that operate at Φ much closer to one. At the same time, advanced combustors are becoming more compact in order to increase the thrust-to-weight ratio [4]. Reduced combustor size typically results in reduced residence time for combustion reactions to complete. These two factors increase the probability of unburned fuel entering the turbine. When the unburned fuel mixes with the oxygen-rich compressor bleed air in the turbine-cooling film, the conditions become right for burning in the turbine. Heat release in the cooling film, whether from recombination of dissociated species or from the combustion of unburned fuel, would drastically reduce the cooling effectiveness of the turbine-cooling scheme and could easily damage the turbine hardware, with potentially severe effects on engine component durability.

Revolutionary gas turbine engine system designs are required in order to meet the conflicting requirements of higher compression ratio, higher peak temperatures, reduced weight, and low emissions, with improved engine durability. The ultracompact combustor (UCC)/interturbine burner currently being developed is one approach to meet this challenge [4,5]. The basis of the concept is to direct the flow of combustion air in the circumferential direction in order to reach sufficient residence times while at the same time reducing the axial length of the component. Figure 1 shows images of a conventional annular combustor (top) and the UCC (bottom).

While a single compact design combining compressor, combustor, and turbine components, which functions synergistically relative to multiple discrete components (like the UCC), would be a tremendous breakthrough in advancing gas turbine engine technology, the UCC presents significant challenges in vane cooling. The high-design fuel-to-air ratio coupled with an increased possibility of fuel-rich streaks residing in a reduced combustor volume with a short length between the combustor and high-pressure turbine (HPT) poses a particularly difficult challenge, as the residence time is typically shorter for mixing and for combustion to complete before reaching the first vane of the HPT. In addition, it is estimated that 10% of the fuel energy, in the form of dissociated species, is available to burn in the turbine sections of the engine [6]. The oxygen-rich film-cooling air can mix and react with the unburned fuel and dissociated species, thus reinitiating combustion in the film-cooling layer adjacent to the surface of the vane. Hence, the air that is intended to provide a protective film and cool the structure could actually have the opposite effect. The challenges presented by this design require a fuller understanding of the interaction between turbine-cooling films and incomplete combustion products and the relationship between boundary layer reactions and the resultant metal temperatures.

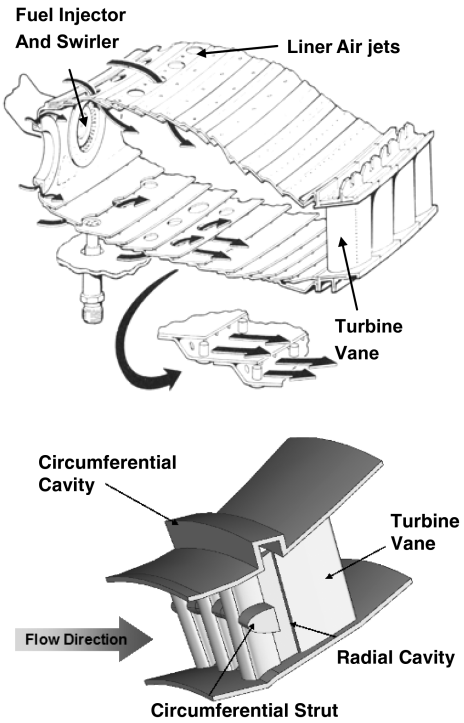

Fig. 1 Conventional axial combustor (top) and UCC (bottom) [4].

Cooling-hole size, shape, and orientation have been previously shown to have a tremendous impact on the cooling effectiveness. This current work's objective is to determine if various film-cooling-hole configurations (circular, angled circular, and fan shaped) result in an increased or decreased likelihood that burning on or near the surface will occur. The experimental database generated as part of this program was used to validate the FLUENT [7] modeling and simulation tools as they are applied to the reactive film-cooling flow studies in this paper. Understanding the fundamental physical processes associated with reaction in the turbine will be accomplished by determining the conditions under which incomplete combustion may permit unburned fuel to reach oxygen-rich film-cooling holes and initiate combustion near the surface of the airfoil. The impact of blowing ratio, equivalence ratio, and cooling-hole shape on the occurrence of heat release on a flat plate geometry are quantified both experimentally and computationally. This research will serve as an incremental step toward the understanding of the physics of reacting boundary layers as they relate to compact combustion systems such as the UCC, in which the turbine vane is integrated into the combustor design. The goal of the research program is to establish a sufficient understanding for the development of turbine-cooling schemes that enable the application of the UCC to future systems.

II. Background

The two primary film-cooling designs used in turbine film cooling are cylindrical holes, either orientated normal or at some surface angle, and a fan-shaped hole, either with or without a layback. The relative benefits of cylindrical, fan-shaped, and laidback fan-shaped holes were studied by Gritsch et al. [8], among many others. The laidback fan-shaped hole has the advantages of ejecting more coolant flow at a lower blowing ratio, thus achieving higher effectiveness. It accomplishes this by increasing the area of the hole near the exit, thus reducing the jet velocity and the tendency of the jet to separate. The benefit of shaping is dramatic, particularly at high blowing ratios.

The potential effect of heat release as a result of secondary combustion occurring due to the air from film-cooling holes was studied by Lukachko et al. [6]. The potential for local temperature rise depended largely on the amount of chemical energy remaining in the flow. The research showed that the local temperature increase in a flow simulating a fuel streak in a future combustor at a stoichiometric fuel-to-air ratio could become large and potentially catastrophic. In a subsequent effort by Kirk et al. [9], a series of shock tube experiments were conducted that examined the impact of near-wall reactions in a cooling film. Their experimental setup allowed concurrent heat flux measurements for a reacting (air) coolant flow and nonreacting (N_2) coolant flow through a 35° injection angle into a freestream mixture of ethylene and argon. Blowing ratios in the test ranged from 0.5 to 2.0, for a range of unburned fuel concentration. At high concentrations of unburned fuel, as much as a 30% increase in heat flux may occur. At moderate CO concentrations, the increase reaches approximately 10%. At low concentrations, the difference between reacting and nonreacting flows is insignificant.

Film cooling operates by protecting the surface from the freestream temperature T_∞ by a flow of coolant at a coolant temperature T_c. The temperature that drives heat transfer is the temperature of the film T_f located adjacent to the surface. Ideally, the coolant ejected from the cooling holes would remain attached to the surface. In this case, T_f would be very close to T_c. This does not in fact occur. The coolant air mixes with the mainstream flow quickly, resulting in a T_f somewhere between T_c and T_∞. This film temperature is difficult to determine experimentally. If an adiabatic wall is generated such that T_f equals T_w, then the performance of the coolant can be quantified by Eq. (2) as follows:

$$\eta = \frac{T_\infty - T_w}{T_\infty - T_c} \tag{2}$$

The computations were performed with an adiabatic wall condition and will be used to reveal the effectiveness of the cooling schemes. However, the experiment was not able to replicate the same adiabatic wall condition, so direct comparisons with the η computations were not possible. Instead, relative comparisons were made to the changes in surface temperature, as will be described in more detail later in the paper.

In this experiment, the chemistry of the flow was also of vital importance. The two main quantities that were of interest were the equivalence ratio and the CO concentration of the flow. The equivalence ratio [given in Eq. (1)] was the ratio of the fuel-to-air ratio for the experiment compared with the same ratio at stoichiometric conditions. For this investigation, propane (C_3H_8) was used as the working fuel, and for the general reaction of propane with air, the stoichiometric fuel-to-air ratio Φ was calculated to be 0.0639. A fuel-to-air ratio higher than this will result in an Φ greater than one and was considered fuel rich. Conversely, any fuel-to-air ratio less than 0.0639 will have an equivalence ratio less than one and is fuel lean.

This study was also interested in how a fuel-rich freestream was influenced by several of the typical film-cooling fluid mechanical parameters. The current study explores a number of them, in addition to the chemistry of the flow. These are the blowing ratio, injection angle, and hole shape. The blowing ratio M, also referred to as the mass flux ratio, is defined as follows:

$$M = \frac{\rho_c U_c}{\rho_\infty U_\infty} \tag{3}$$

where ρU is the product of the density and velocity of the coolant at the hole exit or freestream, respectively. The calculation of M from Eq. (3) directly requires precise knowledge of the density of the gases. The determination of this property in reacting systems is imprecise. Therefore, M was calculated using the conservation of mass. The statement of the conservation of mass for a constant area flow in an incompressible fluid is given in Eq. (4):

$$\frac{\dot{m}}{A} = \rho U \tag{4}$$

Substitution of Eq. (4) into Eq. (3) for both coolant flow and reactor exhaust flow yields the following:

$$M = \frac{\dot{m}_{c,\text{total}} A_\infty}{\dot{m}_\infty A_{c,\text{total}}} \tag{5}$$

Here, $\dot{m}_{c,\text{total}}$ is the total mass flow of the coolant through all cooling holes, $A_{c,\text{total}}$ is the metered area of all cooling holes, A_∞ is the cross-sectional area of the test rig, and $\dot{m}_\infty$ is the mass flow of the reactor exhaust equaling the sum of $\dot{m}_{\text{fuel}}$ and $\dot{m}_{\text{air}}$.

III. Experimental Setup

A well-stirred reactor (WSR), as described by Stouffer et al. [10] and briefly reviewed by Evans et al. [11], was used to simulate the turbine entry conditions of a notional combustor. In the WSR, a high rate of mixing of products and incoming reactants was induced. This results in a nearly uniform distribution of temperature and species within the reactor, at the exit, and within the test section. The mass flow rate and Φ into the reactor were controlled by thermal mass flow controllers.

As outlined by Lukachko et al. [6], the amount of heat release in the flow is a function of the concentration of CO equivalent present in the flow downstream of the combustor. CO equivalent is a measure of the total energy available to cause local temperature rise, determined by the sum of energy content in CO, OH, H_2, O, and HC emissions. In this experiment, a gas sample was fed from the WSR to a standard emissions test bench for characterization of gas concentrations. CO_2 and CO were measured with a California Analytical Instruments Fourier transform infrared spectroscopy analyzer. O_2 was measured with a Horiba magnetopneumatic analyzer. OH was not able to be measured, and the H_2, O, and HC were not measured but assumed to be small compared with the CO, based on Chemkin™ [12] modeling of the reaction revealing that these species were roughly 1% of the CO concentration. Therefore, only the CO was used to compare. The current experiment was performed at ambient pressures that resulted in a slightly different CO concentration at the same Φ as higher (20 atm) pressures. To account for this, Chemkin was run to determine the relative influence on the resultant concentration between the two pressures. At a lower Φ of 0.7 at ambient pressure, the CO concentration is equivalent to that found at an Φ of 0.85 at the elevated pressure. These curves essentially collapse over the range from $1.2 < \Phi < 1.5$ and then diverge again for higher equivalence ratios. This gave confidence that the current ambient pressure results were representative of what would be expected at the elevated pressure. At a Φ of 1.5, the CO percentage was predicted to be about 10.5% and measurements were between 10 and 10.5%, depending on the experiment. This equates to a concentration of 100,000 ppm, which is slightly higher than the Lukachko composition 3. For $\Phi = 0.6$, the measured and predicted concentrations of CO were around 0.35% or 3500 ppm. This is in the range of Lukachko's composition 1. The exhaust of the WSR flows upward through a shaped ceramic chimney, over a forward-facing step that served as a turbulent trip, and into a nominal 5 cm^2 test section. The test surface was a flat plate, and it was enclosed by three quartz window walls. Slots were machined in the plate to allow for the insertion of two cooling air assemblies and four heat-transfer gauge assemblies, as shown in Fig. 2. Each of these assemblies was inserted through the back of the plate, with their surfaces flush with the surface of the plate and fed with cooling air or nitrogen from the facility supply.

The cooling air assemblies were made up of the cooling-hole slot inserts and the plena. The plena were attached to the cooling-hole inserts and sealed with a high-temperature adhesive sealant. In the plena, the cooling pressure was measured with static taps and the air temperature was measured with thermocouples inserted to a location 5.1 mm from the outside surface of the cooling-hole inserts. The cooling-hole geometries were machined into the surface of the inserts. Six different insert geometries were manufactured: normal holes, two rows of offset normal holes, angled holes, fan-shaped laidback holes, angled slot, and a solid blank, as shown in Fig. 3. The normal holes, angled holes, and fan-shaped laidback holes

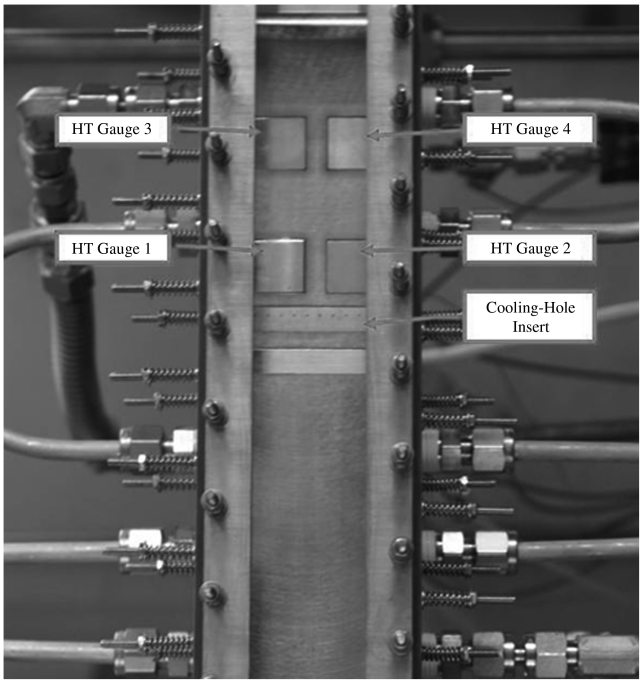

Fig. 2 Flat plate heat-transfer (HT) gauge and cooling-hole insert location.

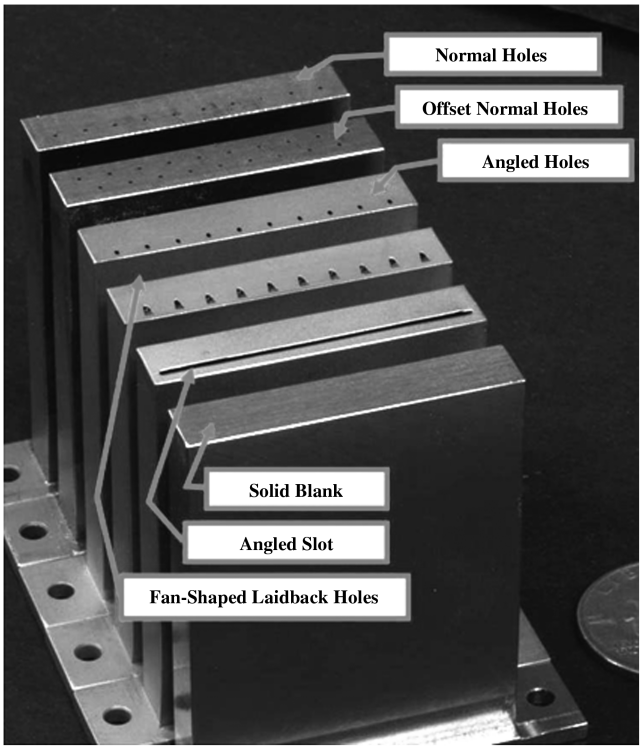

Fig. 3 Cooling-hole insert geometries.

(shaped holes) were studied in this paper. The normal holes were 0.51 mm in diameter, machined perpendicularly through a 2.54 mm surface, giving a hole length-to-diameter ratio (L/D) of five. The spacing between the holes was 3.81 mm. The angled holes were also cylindrical holes of 0.51 mm diameter, but they were machined at an angle of 30° to the surface. To maintain an L/D of five, the surface was necessarily thinner (1.27 mm). The fan-shaped laidback holes were based on the angled-hole geometry, being equal in size, angle, and depth. However, at the surface that sees the flow, the sides of the hole flared out 10°, such that the exit of the hole was 0.91 mm wide. At the same location where the side flares began, the holes were also laidback at the same 10° angle.

To measure the heat transfer and infer the surface temperatures, the four heat-transfer gauge blocks were instrumented with two thermocouples each. A near-surface thermocouple passes through the mount and along a channel cut in the side of the block. It was inserted 11.7 mm into a close-fitting hole that was 3.8 mm from the surface of the block. A second thermocouple was inserted through the bottom of the block to a depth of 19.1 mm from the surface. The thermocouples were at different depths, but the same location measured along the surface. For the two upstream gauges, the thermocouples were 10.4 mm downstream of the cooling holes (approximately 20 hole diameters). The downstream gauges were 38.4 mm downstream (approximately 75 diameters). These thermocouples were positioned a staggered position spanwise between two holes, thus generating an average heat transfer. The surface of the flat plate with all inserts installed was shown in Fig. 2. The film-cooled surface was constructed of Hastelloy-X®, and to maintain the surface at a reasonable temperature, a set of water channels were run through the block. To confirm that the discrete water circuits did not influence the one-dimensional (1-D) conduction in the region of the thermocouples, a typical set of boundary conditions was analyzed with an ANSYS thermal conduction solver. Figure 4 shows the locations of the two water channels that influenced the measurements, the location of the four thermocouples (at the intersections of the lines), and the temperature distribution within the block for a typical set of boundary conditions found in the testing. As the figure shows, the film-cooling plenum had a small influence on the 1-D conduction at the $x/D = 20$ location, the $x/D = 75$ position was purely 1-D, and the water channels did not affect the directionality of the heat transfer at the depth of the thermocouples.

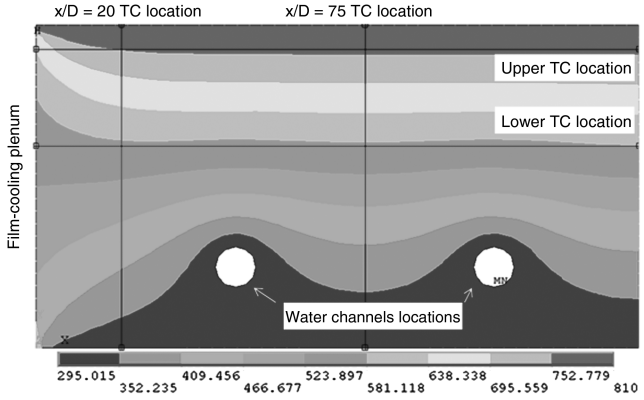

Fig. 4 Thermal analysis of test section (TC denotes thermocouples).

In the current study, the surface temperature of the metal and the heat flux were determined by measuring the temperature using the two thermocouples in a heat-transfer gauge block. The precision error of these temperature measurements was ±0.4%. Assuming 1-D heat transfer, the heat transfer between two thermocouples was calculated for Fourier's law of conduction as follows:

$$q''_x = -k\frac{\mathrm{d}T}{\mathrm{d}x} \tag{6}$$

where q''_x is the heat transfer per unit area, k is the thermal conductivity of the material, T is the temperature in the material, and x is the depth of the thermocouples. Assuming steady-state conditions and 1-D conduction, q''_x is constant, and Eq. (6) can be rearranged and integrated as follows:

$$\int q''_x\,\mathrm{d}x = -\int k\,\mathrm{d}T \tag{7}$$

The temperatures vary from as high as 850 K on the hot surface to as low as 450 K at the deep thermocouple location (1.9 cm from the surface). Over this range, the thermal conductivity varies greatly but in a nearly linear manner. Thermal conductivity can therefore be expressed in the form $k(T) = a_o + a_1 T$, which can be substituted into Eq. (7) and integrated:

$$\frac{a_1}{2}T^2 + a_0 T + q''_x x - C = 0 \tag{8}$$

Here, C is a constant of integration. The heat-transfer gauges provided two thermocouple temperatures, giving two equations that can be used to find q''_x and C. Setting these two equations equal and solving for q''_x gives the equation used to determine the heat flux per unit area:

$$q''_x = \frac{\frac{a_1}{2}(T_1^2 - T_2^2) + a_0(T_1 - T_2)}{(x_2 - x_1)} \tag{9}$$

The precision error calculated was less than 6.2% for q''_x. Substitution of this value back into Eq. (8) using either temperature measurement gives the value of the constant of integration. Once q''_x and C have been found, T_w can be determined from Eq. (8) by setting $x = 0$ and solving the equation for T. A precision error of ±3.3% was found for the uncertainty in T_w.

The primary data that will be discussed in the results section were a relative comparison between the air coolant flow and the nitrogen coolant flow. These two conditions were always obtained on the same day of testing for each configuration, and the order was often alternated as the blowing ratio was varied to ensure that the trends were consistent. Also, a given blowing ratio was occasionally repeated later in the test program to verify that the facility was not changing throughout the testing window. This was done to account for the side-to-side variation measured in the test blocks due to some residual variation within the WSR. Experimentally, the changes between gauges 1 and 3 (as shown in Fig. 2) were consistent with the

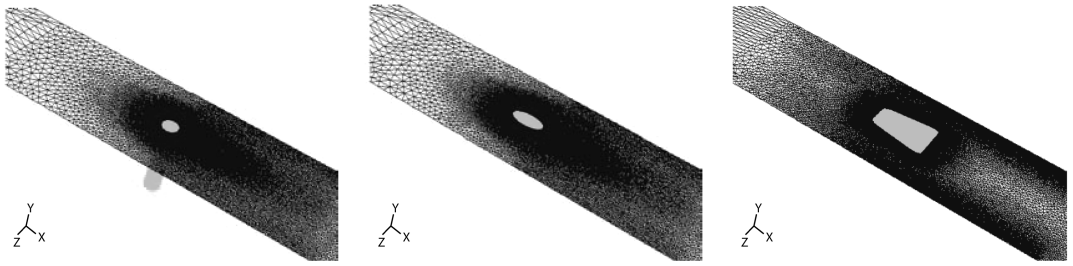

a) b) c)

Fig. 5 Schematic of a) circular normal, b) angled circular, and c) fan-shaped hole meshes.

changes between gauges 2 and 4 within approximately 5 K; gauge 1 could be higher or lower than block 2 by 20 K or more for a given test day or period within a test. What was ultimately verified was that the side-to-side trend in the blocks held true throughout when the results for air were compared with those for nitrogen. An uncertainty of about 1% was measured in surface temperature and subsequent heat flux between repeat points within a test period. A greater variation of closer to 5% occurred in an individual surface temperature, with about a 4% change in the resultant heat flux when trying to reestablish the same condition on a different day. This was often due to changes in the WSR exit stack temperature and/or the coolant exit temperature, which were both difficult to control day to day. However, the difference between the air results and the nitrogen results was consistent, with variation within 2%. To account for some of the overall variation, the results presented are mean values of measurements for gauges 1 and 2 for the 20D location and between gauges 3 and 4 for the 75D location.

IV. Computational Model

This investigation modeled three turbine-cooling-hole designs to provide the information needed to determine under what condition the film of the coolant air combines with the combustor exhaust products causing heat release. The numerical model was based on the FLUENT [7] code. The base finite volume method was used to discretize the governing equations. A pressure-based segregated solver was used with the SIMPLE algorithm for pressure–velocity coupling. A steady implicit Euler scheme was used for the temporal differencing. All equations were spatially discretized using a second-order upwind-differencing scheme, except pressure, which was second order.

The computational domain corresponded to the experimental rig where 10 cooling holes of 0.51 mm in diameter were present. The test rig was symmetric and, initially, a five-hole model was used. Simulations using a single isolated hole followed for the identical conditions, and the results were compared with similar results. Since the pitch ratio of the cooling holes was 7.47, the five-hole model revealed that the jets did not interact until far downstream; therefore, a single-hole mesh with symmetric boundary conditions in the spanwise direction was used for all subsequent simulations. A slip wall boundary condition was used for the top of the domain. Mass flow rate and pressure were specified for the inlet and outlet, respectively. For the cooling hole, mass flow rate of the coolant was specified. The flat surface was treated as an adiabatic wall in the numerical simulation.

The computational model and mesh for the experimental rig with normal circular, angled circular, and shaped holes with a crossflow channel and a plenum are shown in Fig. 5. The measured experimental conditions of pressure, temperature, mass flow, and turbulence level served as the input to a set of perfectly stirred reactor calculations, with Chemkin using a 50 ms residence time. This created the inlet constituents, seen in Table 1, that were used for the computational fluid dynamics (CFD) simulations. Simulations using both nitrogen and air as the cooling fluid have been conducted. The main inlet flow boundary conditions were intended to model the products exiting the combustor and containing unburnt hydrocarbons or other products that may react particularly with the O_2-rich cooling air. These reactions were modeled using a two-step scheme for the propane combustion and described in greater detail in the companion paper [13]:

$$C_3H_8 + 3.5O_2 = 3CO + 4H_2O; \qquad 2CO + O_2 \Leftrightarrow 2CO_2 \quad (10)$$

All of the parameters for the model were the FLUENT default values. This investigation used Reynolds-averaged Navier–Stokes coupled with the shear-stress transport k-ω turbulence model [14] to simulate the turbulent flow. This generated a simple, computationally inexpensive model, and it is expected that a more detailed mechanism may be needed to more accurately model the high equivalence ratio case. The eddy-dissipation-concept model was used to handle the turbulence–chemistry interaction [15]. The calculations were done for a freestream mixture of propane–air vitiated flow at different fuel–air ratios and for various hole shapes. The measured experimental conditions, such as temperature, pressure and mass flow rates for the cross stream and coolant injection, were used to develop the boundary conditions used for the present numerical simulations. The mass fraction of the species at the computational domain's inlet, which corresponds to the exit of a combustor during the experiment, was derived from the experimental setup using the same reaction mechanisms described previously. At first, film cooling with nitrogen injection (without chemical reaction) was modeled. Then, simulation of film cooling with injection of air was conducted. This allowed comparison of the adiabatic cooling effectiveness of N_2 to air. In this paper, calculations were carried out for a freestream mixture of propane–air for equivalence ratios, $\Phi = 0.95$ and 1.5, and a blowing ratio, $M = 1.0$.

A hybrid grid, with both structured and unstructured meshes in selected regions, was employed for the present modeling and simulation. Gridgen V15.10 [16] was first used to create the unstructured surface meshes on a given geometry from a CAD file. The surfaces were loaded into the AFLR grid generator [17,18], which generated the volume mesh from the surface meshes. The mesh was then examined to ensure that there was a minimal amount of equiangular and equivolume skew. Figure 6 shows the computational domain mesh for the five film hole model of the rig and shows the grids used for the fan coolant hole's exit and inlet. Fine grids were generated to resolve the cooling-hole geometry and associated flow physics. Figures 7a–7c show the grid sensitivity effect on the normal circular film hole performance for grids of nearly 2 million cells, over 7 million cells, and over 10 million cells. From interrogation of the flow, there was little variation in the predicted quantities. Hence, the baseline mesh was employed for the results presented in this paper.

V. Results

A. Visible Burning

An extensive test matrix of conditions was performed for the three film-cooling geometries: the normal holes, the angled holes, and the fan-shaped holes. For each geometry, a series of equivalence ratios from 0.6 to 1.7 was tested, and the heat flux was measured over a range of blowing ratios from 0.5 to 2.0. For each condition, two cooling gases were compared to quantify the effect of reaction; namely, air and nitrogen. The nitrogen film serves as the baseline heat

Table 1 Summary of flow conditions

	Pressure, Pa (gauge)	Temperature, K	Mass flow, kg/S	Turbulent, %	C_3H_8	O_2	CO_2	CO	H_2O	N_2
			$\Phi = 0.95$							
Main	1407	1828	5.20e − 04	10	0	1.09e − 02	0.171	0	0.0935	0.72
Air cooling	2169	607	1.35e − 06	1	0	0.23	0	0	0	0.77
			$\Phi = 1.5$							
Main	1407	1837	7.61e − 04	10	0.0296	8.22e − 04	0.176	0	0.0958	0.69
Air cooling	2169	651	2.04e − 06	1	0	0.23	0	0	0	0.77

flux for each condition, and any change that is measured when air is ejected is a direct indication of the heat release due to secondary combustion. Photographs were taken of the angled-hole-cooling geometry at a WSR test condition of $\dot{m}_{\text{air}} = 1020$ g/min and $\Phi = 1.5$. One representative example of these photographs is included as Figs. 8a–8c. The pictures were taken from the side of the rig, with the field of view restricted to the area immediately around the cooling holes. Figure 8a is a photograph of the area of the angled cooling holes with a nitrogen cooling jet at $M = 2.0$. At these conditions, there was no visible flame. Figures 8b and 8c are photographs of the cooling jets with air as the cooling gas. As the air jet meets and mixes with the reactor exhaust flow, the oxygen from the coolant interacts with the fuel in the freestream, and local combustion occurs. The combustion is visible as a white plume as it is carried downstream. These photographs demonstrate that boundary-layer reactions can occur in fuel-rich conditions due to the introduction of air from cooling holes. These reactions happen in close proximity to the surface and occur quickly enough to cause significant heat transfer to the surface in the immediate vicinity of the cooling holes. The pictures were taken with external length references, allowing the length of the plume and penetration to be measured. These measurements indicate that all of the visible reactions occurred within 8 to 16 diameters downstream of the cooling holes. Overall, the higher blowing ratios penetrated deeper, and the plume was longer than lower values of M, as seen when comparing Figs. 8b and 8c. This visible combustion was only seen when the equivalence ratio was higher than 1.0. Tests were run and computations performed at $\Phi = 0.95$, with no indication of localized combustion. For Φ greater than 1.0, though, these reactions were witnessed within the CFD as well as the experiment for all three of the geometries tested.

B. Computational Results

It is important to understand how the film coolant jet interacted with the fuel from the freestream in terms of where the reaction takes place and how impactful that reaction was on the surface temperatures. The coolant jet penetrated into the hot crossflow and induced a pair of counter-rotating vortices, creating three-dimensional (3-D) complex turbulent mixing. For the circular hole normal injection, the film-cooling jet shot out more vertically, penetrating the cross stream with little bending of the jet compared with the angled circular and fanned hole cases, as shown from the thermal contours of the three jet configurations in Figs. 9a–9c. As can be seen in Fig. 8a, at this lower equivalence ratio of 0.95, the normal hole's core was lifted off the surface. The angled-hole temperature core was slightly removed from the surface, but more coolant was present near the wall. In contrast, the fan-shaped-hole core was directly on the wall, resulting in the most effective cooling to the wall. There was not much variation in the temperature field far downstream between the cooling-hole shapes. The nitrogen injection figures for the same conditions are nearly identical at this equivalence ratio, as can be seen in Thornburg et al. [19].

Figure 10 shows the contours of cooling effectiveness on the flat surface under the conditions corresponding to Fig. 9. Again, the air and nitrogen results were nearly identical for this Φ and are not

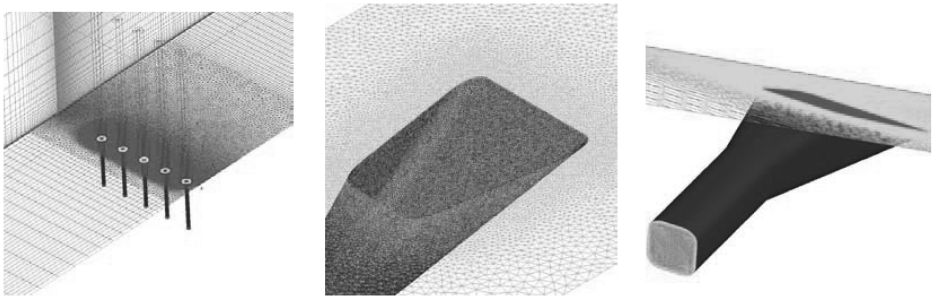

a) b) c)

Fig. 6 Grid schematic of a) five-hole circular hole mesh topology, b) fan-hole exit, and c) fan-hole inlet.

a) Baseline (1,731,368 cells) b) Adapted (7,720,151 cells) c) Uniformly refined (10,504,521 cells)

Fig. 7 Comparison of hole midplane temperature contours (K) for baseline, adapted, and refined mesh.

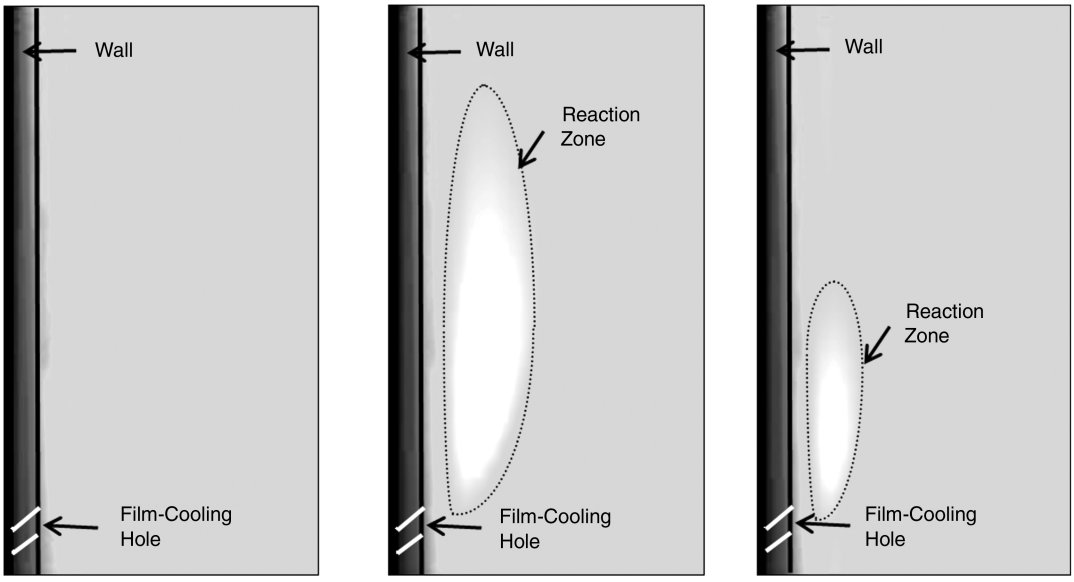

a) Nitrogen, $M = 2.0$ **b) Air, $M = 2.0$** **c) Air, $M = 1.0$**

Fig. 8 Photographs of angled film hole cooling at $\Phi = 1.5$.

shown here, but they can be found in Thornburg et al. [19]. Slightly higher values of cooling effectiveness were found in the area just downstream of the coolant hole, which mimics the basic patterns as observed in conventional nonreactive flow film cooling.

To make this comparison with the literature, Fig. 11 shows the centerline adiabatic effectiveness for a set of 30 cylindrical holes, both with and without a fan shape [8], as compared with the current computational CFD results at $\Phi = 0.95$. The CFD was observed to be lower than the experimental results but followed the same trends. However, the current experiment was performed at an elevated freestream turbulence level around 10%. So the data of Schmidt and Bogard [20] are also shown for an angled-hole geometry in Fig. 10a to display the significant decrease in η that occurs at elevated turbulence, which better brackets the current computational results.

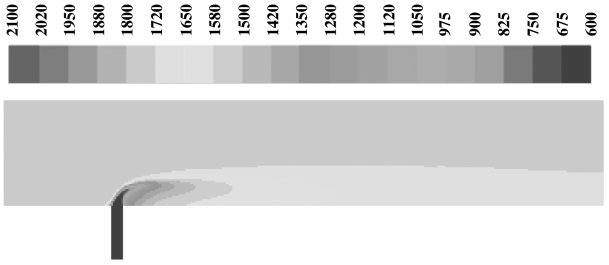

a) Normal circular cooling hole

b) Angled circular cooling hole

c) Fan-shaped cooling hole

Fig. 9 Temperature contours on the midplane for $\Phi = 0.95$, $M = 1.0$, and air injection.

A similar drop would be expected for the shaped holes. This gave confidence that the CFD model was accurately predicting the film-cooling interactions. The experimental results obtained in this study were not adiabatic and, as such, the adiabatic effectiveness was not known.

However, the surface temperatures were determined for each case. These are given in Table 2 at $X/D = 20$ and 75 for $M = 1.0$, and a comparison was made to the computational surface temperatures. Although the differences of the absolute temperatures between simulation and experiment are significant in actual values (due to the heat removal by the water cooling in the experiment), the trends in temperature change were similar between the CFD and experiment. The relative temperature change θ_r is defined:

$$\theta_r = \frac{T_{\text{avg,Air}} - T_{\text{avg,N2}}}{T_{\text{avg,N2}}} \times 100\% \tag{11}$$

where $T_{\text{avg,Air}}$ is the average wall temperature for air injection, and $T_{\text{avg,N2}}$ is the average wall temperature for N_2 injection, both at the same location X/D along flow direction. This parameter allowed comparison between the surface temperature changes that occurred

a) Normal circular cooling hole

b) Angled circular cooling hole

c) Fan-shaped cooling hole

Fig. 10 Adiabatic effectiveness contours on the flat surface for $\Phi = 0.95$, $M = 1.0$, and air injection.

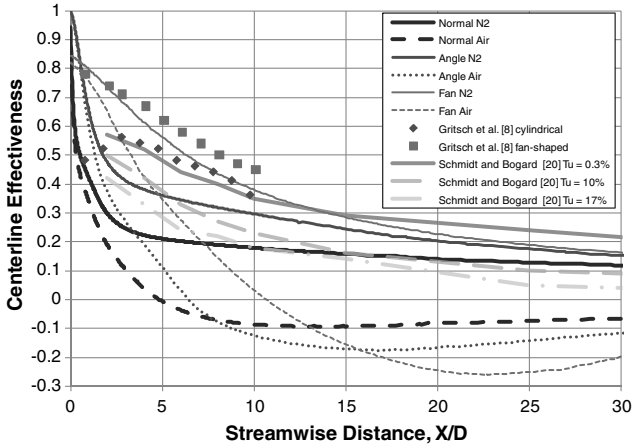

Fig. 11 Experimental centerline adiabatic effectiveness for angled holes from literature compared with current CFD results.

in both the experiment and the computation. In general, rich-burning cases ($\Phi > 1.0$) for air injection generated higher temperatures at a fixed location due to more heat released from combustion, as compared with the lean-burning cases ($\Phi < 1.0$). The CFD showed higher augmentation than the experiment, possibly attributed to only using a two-equation combustion model, but the conditions under which the changes occurred and the relative enhancements were consistent. Both revealed a modest increase for the normal holes, a larger increase for the angled holes, and a significant increase in surface temperature for the shaped holes. The reasons for these trends will be discussed further in the next section. This gives confidence that the simplifications used in this computational method can be extrapolated to other conditions not experimentally tested, and representative results can be expected, especially when temperature change is of concern. As a note, the CFD resulted in surface temperatures that were higher at $X/D = 75$ than at 20, which was expected due to less cooling flow reaching this location. However, in the experiment, the downstream surface temperature decreased due to more water cooling in this regime as compared with upstream.

C. Heat Flux

The experiment was able to reveal the heat transfer to the surface for the various conditions. The values of heat flux at $X/D = 20$ for each of the geometries are compared in Figs. 12a and 12b at representative WSR test conditions. Figure 12a displays q'' for the angled, fan-shaped, and normal holes at $\Phi = 0.95$ and 0.8. The lower equivalence ratio is included to help understand the general trend, as an issue with maintaining the coolant temperature constant was discovered for the fan-shaped-hole configuration at higher blowing ratios, causing those data to be inconsistent. The $\Phi = 0.8$ data were performed at a lower inlet freestream temperature and, as such, the heat flux to the wall was reduced for this condition. However, for both

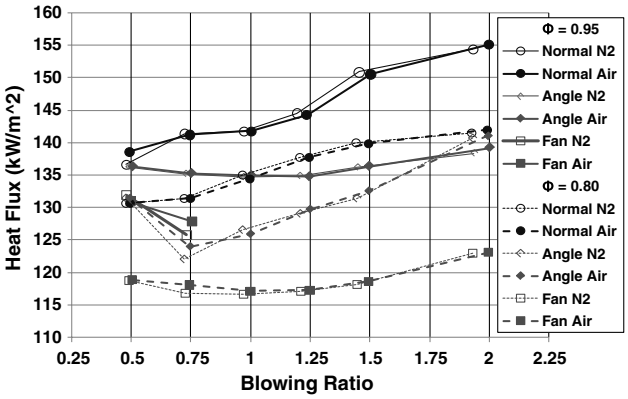

a)

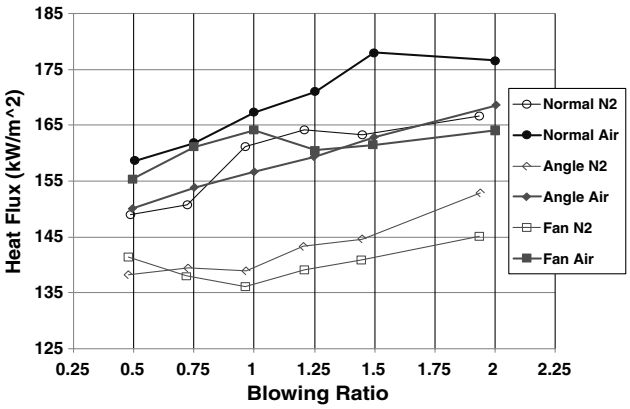

b)

Fig. 12 Heat flux for a) $\Phi = 0.8$ and 0.95 and b) $\Phi = 1.5$.

equivalence ratios, the nitrogen- and air-ejection cases lie nearly on top of each other. The data for cooling air (thick lines) and cooling nitrogen (thin lines) are nearly coincident for each geometry, indicating that boundary-layer reactions had no effect on q'' at these Φ. The angled holes performed better (maintained a lower q'') than the cylindrical holes at lower M, but performance degrades at higher M due to separation. The fan-shaped-hole design provided much lower q'' over the entire range of tested values of M.

Figure 12b shows the q'' data for the cooling geometries at $\Phi = 1.5$. The effect of boundary-layer reactions is clearly seen by the difference between the air (thick lines) and nitrogen (thin lines) data. The dependence of the cooling jets on blowing ratio follows similar trends to those of Fig. 12a. When air is introduced, each geometry indicated a large rise in q''. The q'' of the normal jets increased by an average of 7% when switching from nitrogen to air, while q'' for the angled holes increased by an average of 10%. The fan-shaped holes

Table 2 Comparison of relative temperature changes (θ_r, %) between computations (CFD) and experiments (EXP) for the three-hole configurations

	Conditions		Experimental data			Computational results		
Geometry	Φ	X	$T_{\text{avg,Air}}$, K	$T_{\text{avg,N2}}$, K	θ_r, %	$T_{\text{avg,Air}}$, K	$T_{\text{avg,N2}}$, K	θ_r, %
Normal holes	1.5	20D	823.6	815.1	1.04	1856.53	1727.78	7.45
		75D	749.4	749.0	0.05	1845.09	1747.20	5.60
	0.95	20D	736.3	736.0	0.04	1703.90	1699.50	0.26
		75D	674.2	673.4	0.12	1726.96	1720.93	0.35
Angled holes	1.5	20D	799.5	769.7	3.87	1887.88	1704.57	10.8
		75D	731.5	723.7	1.07	1850.34	1745.53	6.00
	0.95	20D	761.9	761.2	0.09	1683.60	1674.96	0.52
		75D	696.6	696.2	0.06	1725.09	1718.72	0.37
Shaped holes	1.5	20D	813.6	764.7	6.4	1917.40	1686.39	13.70
		75D	739.2	717.5	3.0	1856.46	1738.26	6.80
	0.8 EXP 0.95 CFD	20D	720.2	719.5	0.09	1670.58	1665.04	0.33
		75D	670.7	669.7	0.15	1723.67	1717.09	0.38

(the most effective in the nonreactive flow conditions) increased q'' by 14%. Interestingly, the shape of the curve changed for the fan-shaped holes. The value of q'' when at $M = 1$, precisely where it reaches a minimum in a nonreactive case, has increased by 25% to one of the highest levels of q''. This indicates that the phenomenon that makes the fan-shaped holes characteristically so effective, a resistance to separation, may be increasing the effect of heat release in a reacting flow. This was essentially confirmed by the computational results. As shown previously in Fig. 9, the jets remain closer to the airfoil surface for the fan-shaped hole. Now, in the presence of unburned fuel, any reaction that occurred would also happen closer to the wall. This caused more heat release near the wall and thus higher temperatures. These high temperatures were the source of the elevated heat transfer. For air injection, the cooling air reacted with the chemical species in the crossflow, releasing heat that altered the thermal flowfield and increased the heat transfer as compared with N_2 injection. Each of these cases had a WSR exit temperature of about 1840 K and a similar CO concentration around 10%. This emphasizes that it is the amount of fuel in the flow that influences the reaction. The companion paper [13] will take a deeper look into where the fuel is located and how it is consumed.

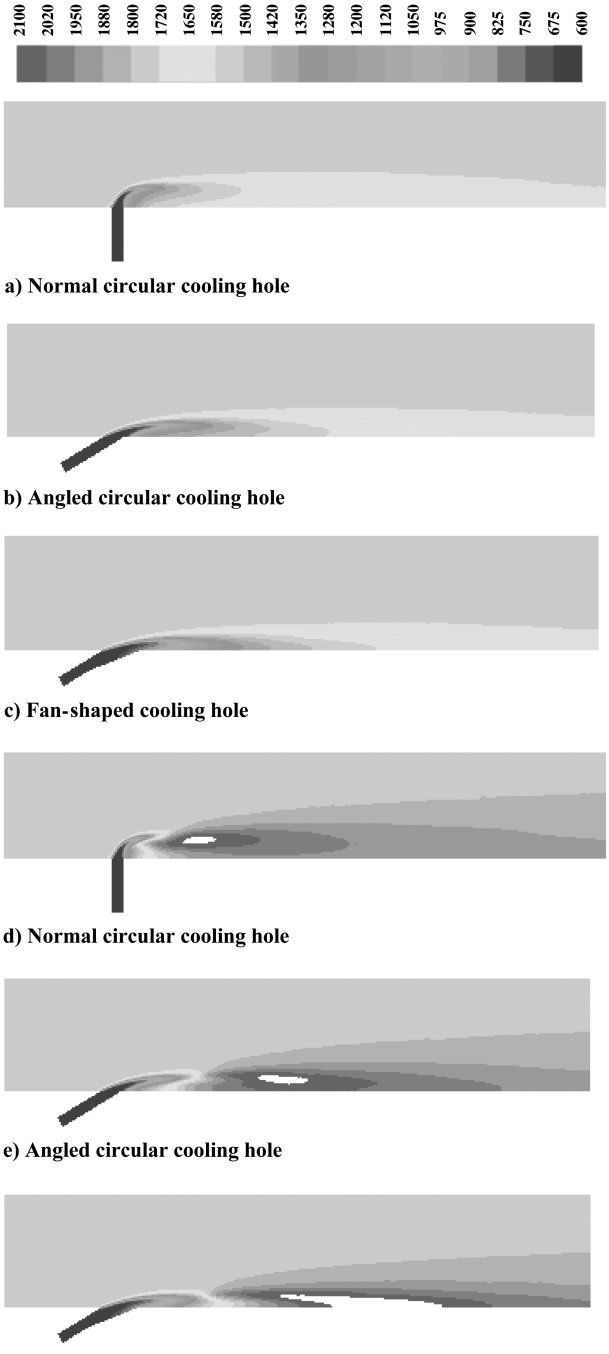

Fig. 13 Temperature contours on the midplane for $\Phi = 1.5$ and $M = 1.0$: a–c) N_2 injection and d–f) air injection.

D. Fuel-Rich Cases

The thermal field for the fuel-rich case, $\Phi = 1.5$, is displayed computationally in Fig. 13. The nitrogen-injection cases, shown in Figs. 13a–13c, are comparable to those seen previously at $\Phi = 0.95$ (Fig. 9). Compared with the N_2-injection cases, however, the secondary combustion in the air-injection cases generates a hot area downstream of the cooling layer near the flat surface (Figs. 13d–13f). In fact, this hot area cuts short the productive portion of the cooling layer downstream of the coolant hole. At the elevated equivalence ratio, the coolant was replaced with a higher-than-freestream temperature region. The location and extent of this high-temperature region changed for the different geometries. For the normal circular hole, the peak temperature was off the surface and was limited in extent. For the angled hole, the location was further downstream, closer to the surface and longer in extent. The worse condition was for the fanned hole, as here, the peak temperature was located directly on the airfoil surface and was significantly larger. This was the cause of the elevated heat flux levels, shown in Fig. 12b.

Figure 14 shows the typical cooling effectiveness on the flat surface for N_2 and air injections at $\Phi = 1.5$. For the cases of N_2 injection, the cooling effectiveness patterns were similar, with the area of the higher level of cooling effectiveness right downstream of the coolant hole. In general, angled circular and fanned holes performed better in terms of increased cooling effectiveness compared

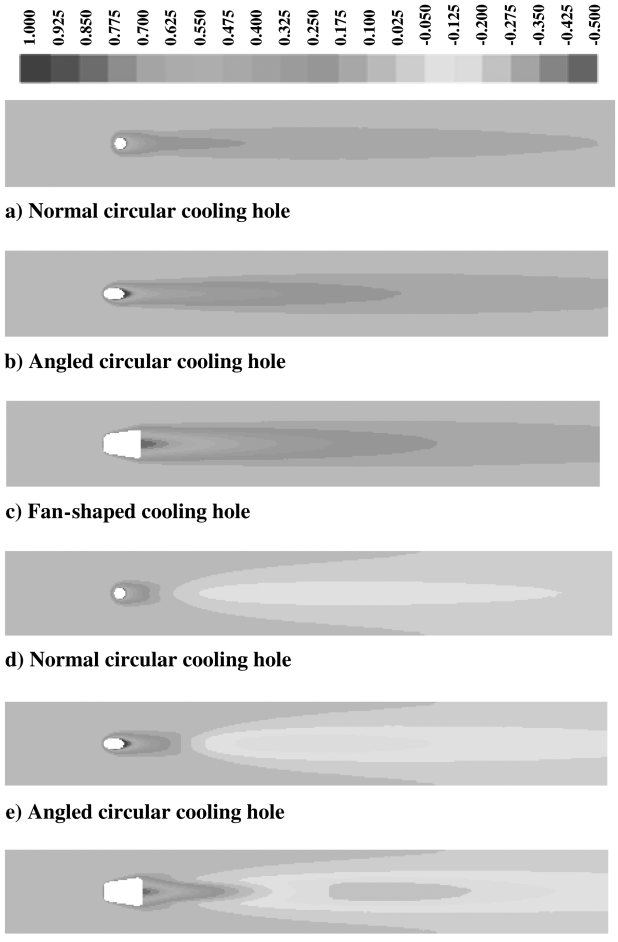

Fig. 14 Cooling effectiveness contours on the flat surface for $\Phi = 1.5$ and $M = 1.0$: a–c) N_2 injection and d–f) air injection.

with the normal circular hole. For cases with air injection, in addition to the area of higher level of cooling effectiveness right downstream of the coolant hole, a zone with negative values of cooling effectiveness appears further downstream. This was attributed to the elevated surface temperature, shown in Fig. 13, causing the adiabatic wall temperatures for these cases with reaction to be higher than the incoming freestream temperature. In classic literature on film cooling, the cooling effectiveness value is always positive, because there is no reaction to add additional heat to raise the wall temperature above the freestream temperature. Based on the traditional definition of adiabatic effectiveness, given in Eq. (1), having an elevated adiabatic wall results in values of η less than 0.0. The location of the negative cooling effectiveness zone corresponds to the hot area due to the secondary combustion. With the fan-shaped hole maintaining the coolant closer to the surface, the cross-stream mixing occurs closer to the surface, causing increased chemical reactions and thus a large region of negative effectiveness downstream. Therefore, the cooling design that was most effective at low Φ (the shaped holes) can potentially have the worst performance at elevated Φ. The ability of these holes to keep the coolant flow close to the surface, which is beneficial at low Φ, also results in the oxygen remaining close to the surface. This results in chemical reactions, and thus the highest thermal load happening in the worst possible location. This ultimately suggests that avoiding standard film cooling completely could be more beneficial from a durability point of view than injecting the typical air flow from film holes. The negative cooling effectiveness is one of the major unique characteristics in reactive flow film cooling, a subject deserving special attention from researchers. There are certainly alternatives to overcome this issue, from material changes to interior cooling configurations, to possibly injecting with alternative gases that do not react, which all need further research.

Figure 15 shows the temperature distribution on the wall along the lateral direction at selected axial stations; namely, $X/D = 5$, 10, 20, and 75. At $X/D = 5$, the liftoff of the jets was apparent, as reacting flow has already convected underneath the jet, thus raising the surface temperature. Conversely, the shaped-hole coolant remained attached, and the surface temperature was reduced by the presence of the coolant. At $X/D = 10$, the normal hole configuration had a similar temperature rise as at $X/D = 5$, as the coolant was fully separated from the wall. While not a beneficial condition, it was better than the angled-hole case, as the reactions were occurring closer to the wall, thus resulting in a 200 K increase in the surface temperature. For the shaped holes, the reactions are occurring along the coolant edges, as that is where the highest mixing was occurring, creating the two-lobed temperature distribution. This changed by $X/D = 20$, as the jet continued to spread, bringing more fuel into the core of the jet; thus, the reaction now peaks along the centerline. This results in nearly a 350 K rise in surface temperature for this condition.

The angled holes have a 200 K rise, and the normal holes still increase only about 100 K. By $X/D = 75$, the film air was mostly reacted with the freestream vitiates, causing a general 50 K increase for each film-cooling condition.

Comparing these results at $\Phi = 1.5$ to the published literature reveals the significance of the drop in effectiveness, as shown in Fig. 16. This figure shows the laterally averaged effectiveness for both air and nitrogen ejections as compared with the experimental results of Pederson et al. [21] and Baldauf et al. [22], both using angled circular holes. When nitrogen was used as the coolant, the CFD (averaged over the same pitch spacing of 3-D as the

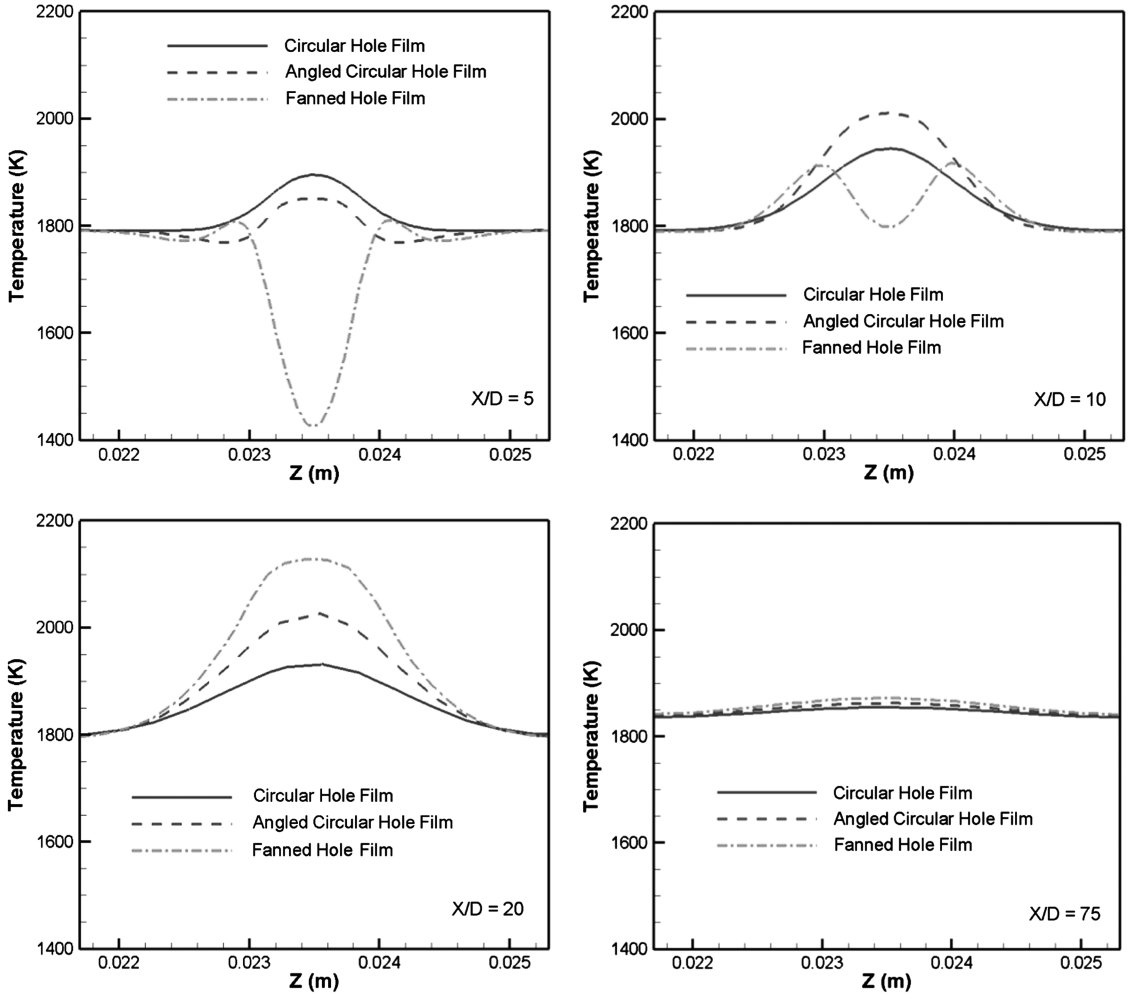

Fig. 15 Spanwise temperature profiles at selected axial locations downstream of the holes.

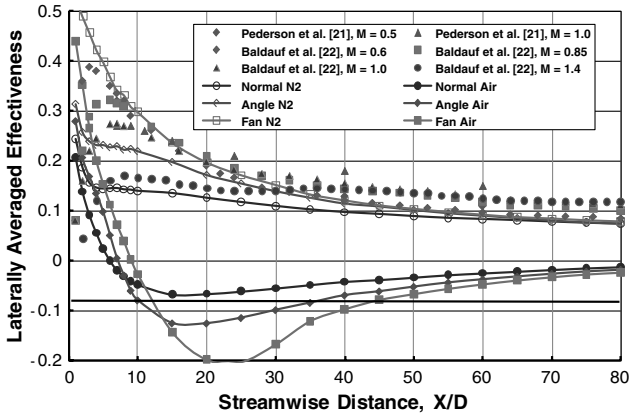

Fig. 16 Comparison of current high equivalence ratio effectiveness to Pederson et al. [21] and Baldauf et al. [22].

experimental data) follows the general results from the experimental data, with the fan-shaped hole having slightly better performance and the normal hole somewhat lesser benefit. The biggest discrepancies were right near the holes and far downstream. This is due in part to the higher turbulence in the current investigation compared with the experimental results. However, with air injection, η significantly dropped and even became negative in the locations of high heat release. The decrease in effectiveness occurs very quickly, but it has its most significant impact between $X/D = 10$ and 20, as shown in Fig. 14. Clearly, these reactions significantly impact the benefits of film cooling and will need to be of concern as higher equivalence ratio combustors are used in the future.

VI. Conclusions

In this study, the impact of heat release in turbine film cooling was explored; specifically, the interaction of cooling flow with the exhaust of a fuel-rich WSR operating at high temperatures over a flat plate. A test rig was designed and constructed with modular components to allow different cooling-hole geometries to be studied. The cooling holes were supplied with either air or nitrogen, allowing the effect of reactions to be isolated. The design of the rig will also support follow-on studies that will use laser diagnostics and high-temperature thin film gauge arrays to further explore the impact of heat release. Surface temperatures and heat flux were calculated for a variety of reactor fuel-to-air ratios, cooling-hole geometries, and blowing ratios. These results were analyzed and compared with CFD calculations of the same conditions. The CFD provided for calculation of the adiabatic effectiveness that was not able to be obtained in the experiment.

The mixing of oxygen-rich turbine-cooling air with a combustor exhaust stream containing unburned fuel resulted in reactions occurring in the cooling film. These reactions occurred close to the surface and resulted in augmented heat transfer to the metal. The magnitude of the increase in heat transfer was driven by the fuel content of the combustor exhaust stream, the blowing ratio, and the geometry of the cooling holes. There was no indication in this study that augmented heat transfer occurred at fuel-to-air ratios less than stoichiometric. The results indicated that the fan-shaped holes provided a lower heat transfer and higher adiabatic effectiveness at all nonreacting test conditions, consistent with the literature. However, the presence of fuel in the exhaust stream seriously degraded the performance of this configuration, resulting in the highest effective heat transfer and the largest areas of negative adiabatic effectiveness for some blowing ratios. This was attributed and shown to be a result of reactions occurring near the surface, resulting in higher local driving temperatures than the upstream freestream temperature. A turbine-cooling scheme designed to take advantage of the improved performance of the fan-shaped holes in a nonreactive condition could underpredict the magnitude of augmented heat release due to fuel streaks, potentially resulting in severe turbine durability degradation. This investigation and these results set the groundwork for continued development of new combustor schemes like the UCC, where the possibility for unburnt species to be present in the turbine section exists.

Acknowledgments

The authors wish to acknowledge Paul King from the Air Force Institute of Technology for his thoughtful oversight of this effort. We also appreciate the efforts of Chuck Abel of Innovative Scientific Solutions, Inc., and Mike Arstingstall of the University of Dayton Research Institute (UDRI) for their assistance in machining the test pieces and running the experiments, respectively. The authors also acknowledge David Bogard from the University of Texas for his aide with regenerating the experimental data used from the literature. Also needing acknowledgement are Alejandro Briones from UDRI and Hugh Thornburg from Mississippi State University for their work on portions of the computational effort needed for this paper.

References

[1] Ballal, D. R., and Zelina, J., "Progress in Aero Engine Technology (1939–2003)," AIAA Paper 2003-4412, 2003.

[2] Bogard, D. G., and Thole, K. A., "Gas Turbine Film Cooling," *Journal of Propulsion and Power*, Vol. 22, No. 2, 2006, pp. 249–269. doi:10.2514/1.18034

[3] Mattingly, J. D., Heiser, W. H., and Daley, D. H., *Aircraft Engine Design*, AIAA, Washington, D.C., 1987.

[4] Zelina, J., Sturgess, G. J., and Shouse, D. T., "The Behavior of an Ultra-Compact Combustor (UCC) Based on Centrifugally Enhanced Turbulent Burning Rates," AIAA Paper 2004-3541, 2004.

[5] Zelina, J., Shouse, D. T., and Hancock, R. D., "Ultra-Compact Combustors for Advanced Gas Turbine Engines," American Soc. of Mechanical Engineers Paper 2004-GT-53155, Fairfield, NJ, 2004.

[6] Lukachko, S. P., Kirk, D. R., and Waitz, I. A., "Turbine Durability Impacts of High Fuel-Air Ratio Combustors, Part 1: Potential For Intra-Turbine Oxidation of Partially-Reacted Fuel," *Presented at ASME Turbo Expo 2002: Land, Sea and Air*, Amsterdam, American Soc. of Mechanical Engineers Paper 2002-30077, Fairfield, NJ, 2002.

[7] FLUENT Ver. 6.3.26, Software, Fluent, Inc., Ann Arbor, MI, 2007.

[8] Gritsch, M., Schulz, A., and Wittig, S., "Adiabatic Wall Effectiveness Measurements of Film-Cooling Holes with Expanded Exits," *Journal of Turbomachinery*, Vol. 120, No. 3, July 1998, pp. 549–556.

[9] Kirk, D. R., Guenette, G. R., Lukachko, S. P., and Waitz, I. A., "Gas Turbine Engine Durability Impacts of High Fuel–Air Ratio Combustors Part 2: Near Wall Reaction Effects on Film-Cooled Heat Transfer," *ASME Turbo Expo 2002: Land, Sea and Air*, Amsterdam, American Soc. of Mechanical Engineers Paper 2002-30182, Fairfield, NJ, 2002.

[10] Stouffer, S. D., Striebich, R. C., Frayne, C. W., and Zelina, J., "Combustion Particulates Mitigation Investigation Using a Well-Stirred Reactor," AIAA Paper 2002-3723, 2002.

[11] Evans, D., King, P., Polanka, M., Zelina, J., Anderson, W., and Stouffer, "Impact of Heat Release in Turbine Film Cooling," 46th AIAA Aerospace Sciences Meeting and Exhibit, Orlando, FL, AIAA Paper 2009-0298, Jan 4–8, 2009.

[12] Kee, R. J., "CHEMKIN Release 4.1.1," Reaction Design, San Diego, CA, 2007.

[13] Lin, C. X., Holder, R. J., Sekar, B., Zelina, J., Polanka, M. D., Thornburg, H. J., and Briones, A. M., "The Impact of Heat Release in Turbine Film Cooling, Part II: Numerical Simulation of Shaped Hole Secondary Combustion Development and Location," *Journal of Propulsion and Power*, Vol. 27, No. 2, 2011, pp. 269–281. doi:10.2514/1.45318

[14] Menter, F. R., "Two-Equation Eddy-Viscosity Turbulence Models for Engineering Applications," *AIAA Journal*, Vol. 32, No. 8, 1994, pp. 1598–1605. doi:10.2514/3.12149

[15] Magnussen, B. F., "On the Structure of Turbulence and a Generalized Eddy Dissipation Concept for Chemical Reaction in Turbulent Flow," 19th AIAA Aerospace Sciences Meeting, St. Louis, MO, AIAA Paper 1981-0042, 1981.

[16] Gridgen Ver. 15, Software, Pointwise, Inc., Fort Worth, TX, 2004.

[17] Marcum, D. L., and Weatherill, N. P., "Unstructured Grid Generation Using Iterative Point Insertion and Local Reconnection," *AIAA Journal*, Vol. 33, No. 9, Sept. 1995, pp. 1619–1625. doi:10.2514/3.12701

[18] Marcum, D. L., "Unstructured Grid Generation Using Automatic Point Insertion and Local Reconnection," *The Handbook of Grid Generation*,

edited by J. F. Thompson, B. Soni, and N. P. Weatherill, CRC Press, Boca Raton, FL, 1998, p. 18-1.
[19] Thornburg, H., Sekar, B., Zelina, Z., Anderson, W., Polanka, M. D., Lin, C. X., Holder, R. J., Briones, A. M., and Stouffer, S. D., "Design Studies of Turbine Blade Film Cooling with Unburned Fuel in Cross Stream Flow," AIAA Paper 2009-0510, 2009.
[20] Schmidt, D. L., and Bogard, D. G., "Effects of Free-Stream Turbulence and Surface Roughness on Film Cooling," American Soc. of Mechanical Engineers Paper 96-GT-462, Fairfield, NJ, 1996.
[21] Pedersen, D. R., Eckert, E., and Goldstein, R., "Film Cooling with Large Density Differences Between the Mainstream and the Secondary Fluid Measured by the Heat-Mass Transfer Analogy," *Journal of Heat Transfer*, Vol. 99, No. 4, 1977, pp. 620–627. doi:10.1115/1.3450752
[22] Baldauf, S., Scheurlen, M., Schulz, A., and Wittig, S., "Correlation of Film-Cooling Effectiveness from Thermographic Measurements at Engine like Conditions," *Journal of Turbomachinery*, Vol. 124, No. 4, 2002, pp. 686–698. doi:10.1115/1.1504443

C. Tan
Associate Editor